Eur. Phys. J. A **21**, 391–406 (2004)
DOI 10.1140/epja/i2003-10224-x

THE EUROPEAN PHYSICAL JOURNAL A

Fission barriers of heavy nuclei within a microscopic approach

L. Bonneau[a], P. Quentin, and D. Samsœn

Centre d'Etudes Nucléaires de Bordeaux-Gradignan, CNRS-IN2P3 and Université Bordeaux-I, BP 120, F-33175 Gradignan, France

Received: 20 June 2003 / Revised version: 9 March 2004 /
Published online: 21 September 2004 –
Communicated by A. Molinari

Abstract. The fission barriers of twenty-six isotopes of Thorium, Uranium, Plutonium, Californium, Fermium and Nobelium have been microscopically calculated up to and beyond the second saddle point within a constrained Hartree-Fock plus pairing approach. The Skyrme density-dependent effective force in its SkM* parametrization —rather well suited to the description of fission barriers— has been used in the particle-hole channel, whereas the usual HF plus BCS formalism with either a seniority force or a delta force has been implemented to treat pairing correlations. The energy correction due to the rotational zero-point motion has been approximately taken into account and the effects of triaxial and reflection asymmetric deformations have been investigated. When known, the experimental fission barrier heights are reproduced within about 1–2 MeV.

PACS. 21.60.Jz Hartree-Fock and random-phase approximations – 24.75.+i General properties of fission

1 Introduction

A correct microscopic description of first and second fission barriers of actinide or heavier isotopes is well known to be strongly and equally contingent upon two different theoretical ingredients. Specifically, one needs a correct reproduction of the behaviour of both the bulk and the shell correction energies with respect to the relevant collective mode parameters (mostly the elongation, at least at the beginning of the process). Indeed, in the considered deformation range, the variation of these two ingredients of the total energy (in the sense of the Strutinsky truncated expansion scheme [1]) are of the same order of magnitude, namely some MeV, as functions of the deformation (assuming a good reproduction of the underlying liquid-drop model properties). The same good assessment of shell correction energies is also crucial in predicting the stability properties of superheavy species. In this context, in so far as the corresponding fission barrier heights are known experimentally, computing realistic deformation energy curves for very heavy nuclei constitutes undoubtedly a demanding double test for any effective interaction to be used in the calculation of the properties of superheavy nuclei. This is why we have tried to reproduce fission barriers of well studied (theoretically [2–13] and experimentally [14–17]) Thorium, Uranium and Plutonium isotopes within a fully microscopic mean-field approach. Recently, results of relativistic mean-field calculations have even been made available [18,19]. Taking stock on the success of this attempt, we have computed fission barriers of three isotopic series of very heavy even-even nuclei in the region $Z = 100$. Some of the nuclei considered here have also been studied in recently published theoretical calculations by another group [20].

Section 2 will be devoted to a brief account of the theoretical framework with special attention paid to numerical developments which have warranted the numerical convergence of the present approach and extended its grasp in the collective variable space as compared to previous comparable attempts [10]. Our results will then be presented and discussed in sect. 3, while conclusions will be drawn in sect. 4.

2 Theoretical framework and numerical aspects

Our approach relies on Hartree-Fock (HF) plus BCS codes developed in ref. [21] for axially symmetrical solutions, and ref. [22] for triaxial solutions with a Skyrme force. As will be discussed later, we have extended the former code in order to allow for a breaking of the reflection symmetry about an equatorial plane. A word of caution is worth adding at this point. What is generally dubbed as "axial symmetry" should be more likely be referred to as "revolution symmetry". In the same spirit, "triaxial symmetry" arising from breaking this revolution symmetry corresponds in fact to "ellipsoidal symmetry", namely

[a] e-mail: bonneau@lanl.gov

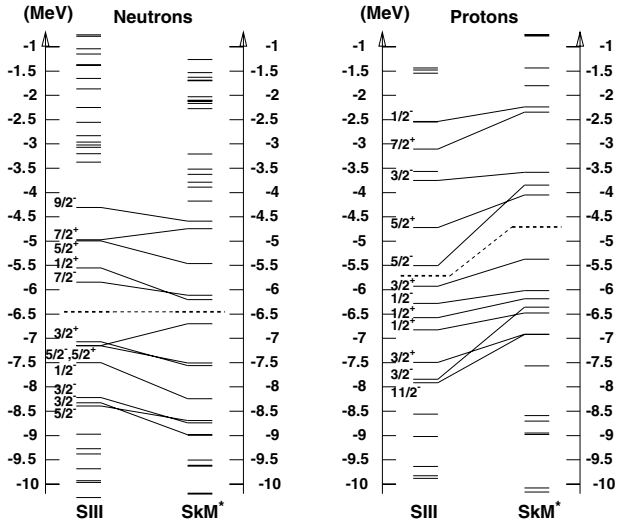

Fig. 1. Single-particle spectra of ^{234}U with SIII and SkM* Skyrme interactions for the ND minimum. The Fermi levels are indicated with dashed lines.

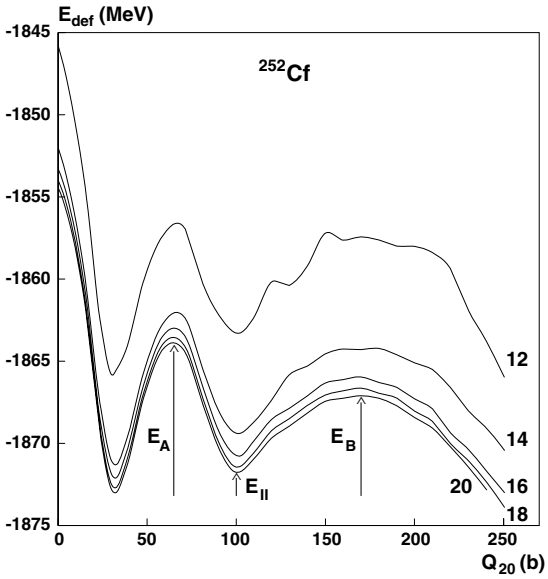

Fig. 2. Deformation energy curves of ^{252}Cf for different N_0-values within HF + BCS(G) approach. From top to bottom the curves correspond to $N_0 = 12$, $N_0 = 14$, $N_0 = 16$, $N_0 = 18$ and $N_0 = 20$ (see sect. 2.2).

a symmetry with respect to the three principal planes. In these codes, even when breaking the axial symmetry of the solutions, the single particle HF wave functions have been expanded onto an axially symmetrical deformed harmonic-oscillator truncated basis. Owing to the zero range (plus simple corrective terms) of the Skyrme interaction, the total energy appears as an energy density functional. All relevant numerical integrations have been performed within Gauss methods, whose orders have been explicitly revisited in view of the very large deformations considered here.

The SkM* parametrization [11] has been chosen for the Skyrme force. Its underlying surface tension properties have been explicitly adjusted to the liquid-drop fission barrier of ^{240}Pu from the original SkM parametrization [23]. This makes it *a priori* suitable for fission barrier calculations as opposed, for instance, to the SIII [24] parametrization shown in ref. [25] to correspond to a too high value of the surface tension parameter. However, as discussed in the introduction, it remains to be checked that the single particle (sp) properties resulting from the use of the SkM* force are good enough. In this domain, a good reference within the usual Skyrme parametrizations is precisely the SIII force. Indeed it has been shown in various nuclei and at various deformations (see, *e.g.*, the extensive study of sp configurations in the ^{235}U ground state [26], the study of isomeric properties of the ^{178}Hf [27] or the fission isomer spectroscopy in odd compound systems [28]). We have therefore assessed the value of the sp properties obtained in HF plus BCS calculations using the SkM* force by comparing them with what is yielded with the SIII force. For instance, in fig. 1, the neutrons and protons spectra obtained in the ground state of ^{234}U have been compared for both forces. It appears that, while some reordering of given sp states is sometimes experienced from one calculation to another, the sp level densities near the chemical potentials, which are the relevant quantities in a Strutinsky approach, are found to be quite similar. As a result, in view of the excellent quality of the liquid-drop properties and the reasonable sp level densities associated with the SkM* force, we have deemed that such an effective interaction could constitute a suitable Skyrme force parametrization for our purpose.

2.1 Numerical aspects

The axially symmetrical harmonic-oscillator basis must obviously be truncated. As done in ref. [21], the truncation prescription uses the following deformation-dependent energy cut-off:

$$\hbar\omega_\perp(n_\perp + 1) + \hbar\omega_z\left(n_z + \frac{1}{2}\right) \leqslant \hbar\omega_0(N_0 + 2). \qquad (1)$$

It introduces, for a given basis size N_0, a spurious dependence of computed physical quantities on basis parameters b and q defined by [21]

$$b = \sqrt{\frac{m\,\omega_0}{\hbar}}\,, \qquad q = \frac{\omega_\perp}{\omega_z}\,, \qquad (2)$$

where m is the mass of the nucleons (which is approximated as being equal for neutrons and protons). In view of the variational character of our approach, we have therefore fixed those parameters for each deformation point and each nucleus to their values minimizing the energy.

We have studied the convergence of our results as a function of the basis parameter N_0. Clearly, upon increasing the basis size, the energy should be lowered. However,

Table 1. Energies (in MeV) of the first barrier E_A, the superdeformed minimum $E_{\rm II}$ and the second barrier E_B, respectively of ^{252}Cf relative to the normally deformed minimum obtained with different N_0-values.

N_0	E_A	$E_{\rm II}$	E_B
12	10.8	2.5	8.6
14	10.9	1.9	7.1
16	10.1	1.3	6.0
18	10.2	1.3	6.1
20	10.2	1.2	5.9

Table 2. HF+BCS(G) fission barrier heights evaluated within two different basis optimization processes (without rotational correction). For each nucleus, the first line corresponds to the optimization with $N_0 = 14$ and the second one, with $N_0 = 16$.

	E_A		E_B	
Nucleus	axial	triaxial	symmetric	asymmetric
	7.9	7.6	12.6	6.5
^{236}U	7.7	7.5	12.5	6.3
	10.1	8.1	6.0	5.0
^{252}Cf	9.8	8.3	6.2	5.2

since a fission barrier carries a physical information only on relative energies (deformation energies), it is sufficient to prove that these energy curves are merely translated downwards when increasing N_0 in the relevant range of this parameter. As shown in fig. 2 and in table 1, this is the case in the typical example of the fission barrier of ^{252}Cf, for $N_0 \geqslant 16$.

Therefore, in what follows, we have performed all calculations with $N_0 = 16$, except the optimization of basis parameters which has been performed with $N_0 = 14$ for computation time reasons. Nevertheless, it has been checked on two nuclei (^{236}U and ^{252}Cf) that the barrier heights obtained with $N_0 = 16$ after a $N_0 = 14$ optimization differ by less than 0.3 MeV from what would have been found within a full $N_0 = 16$ calculation (see table 2 for the barrier heights as functions of the optimization process in some axial cases). It is to be noted that recent Hartree-Fock-Bogoliubov calculations of fission barriers in the Fm region of ref. [20] using the D1S parametrization of the Gogny force also find converged results beyond the second barrier around $N_0 = 16$.

Furthermore, a particular attention has been paid to the numerical accuracy of the Gauss quadratures at very large deformation which had impaired previous attempts [10] beyond the fission isomeric (secondary minimum) state. Three different Gauss methods have been used:

– along an axis perpendicular to the basis state symmetry axis, we have used a 16-points Gauss-Laguerre approach;

– while most of the azimutal angle integrations have been simply dealt within a Fourier decomposition [22], a Gauss-Legendre formula with 50 points has been used for the elliptic-like integrals involved in the Coulomb field calculations;

– along the basis state symmetry axis, a Gauss-Hermite quadrature using 50 points (which reduces to twice 25 points for left-right reflection symmetrical integrands) has been considered.

The latter choice has been shown to be crucial in yielding a reasonable numerical accuracy. Indeed, upon increasing the basis parameter q, one includes through the truncation scheme imposed by eq. (1), basis states with higher and higher number of nodes on this axis. It has appeared that the order of the Gauss-Hermite method should be accommodated to the corresponding maximal n_z-values. The retained value (50) has been shown to be sufficient for $N_0 \leqslant 20$ up to the larger deformations under consideration here (far beyond the second saddle point).

2.2 Pairing treatment

To take neutron-neutron and proton-proton pairing correlations into account, we have used the usual BCS approximation with two different pairing interactions: the seniority force (yielding calculations referred to as HF+BCS(G) in the following) and a δ-force (with corresponding calculations referred to as HF + BCS(δ)). The strengths g_q (where q is a charge state index) of the first one have been fitted to reproduce the moments of inertia and the transition energies between some low spin states in the ground-state rotational band of ^{254}No [29]. The retained values are

$$g_q = \frac{G_0^{(q)}}{11 + N_q} \ \text{(MeV)} \tag{3}$$

with $G_0^{(n)} = 14.3$ MeV for neutrons and $G_0^{(p)} = 15.5$ MeV for protons and where N_q are the corresponding nucleon numbers. Together with these values for the strength, we have used a sp configuration space defined by a sharp energy cut-off of 6.2 MeV above the Fermi level for both charge states.

As for the δ-force, the strength parameters were fitted to reproduce the energies of the isomeric states in the A $\sim$ 178 region [30]. They are given by (in the notations of ref. [31]) $V_{00}^{(n)} = -386$ MeV and $V_{00}^{(p)} = -498$ MeV. In this case we have used a soft boundary cut-off defined, with the notations of ref. [27], by $X = 6$ MeV and $\mu = 0.2$ MeV. The matrix elements of the residual δ-interaction have been evaluated by Gauss quadratures using the same numbers of integration points as above discussed.

2.3 Rotational correction

Due to a preferential orientation in space of the intrinsic ground state, a rotational zero-point motion correction has been taken into account. It has been performed *à la* Lipkin [32,33] assuming thus a perfect rotational character for the rotational band which would be obtained when projecting, namely

$$E_{\rm rot} = \frac{\langle \hat{J}^2 \rangle}{2\,\mathcal{I}_{\rm Bel}}\,, \tag{4}$$

where $\mathcal{I}_{\rm Bel}$ is the moment of inertia calculated according to the Belyaev formula [34], so that the total energy of the 0^+ state is approximately related to the intrinsic energy by

$$E_0 \approx E_{\rm intr} - E_{\rm rot}\,. \tag{5}$$

We have chosen to compute both the moment of inertia $\mathcal{I}_{\rm Bel}$ and $\langle \hat{J}^2 \rangle$ in a consistent way. This has been achieved within the HF+BCS approximation as described, *e.g.*, in ref. [35] only within the axial symmetry. The expression (4) of $\langle \hat{J}^2 \rangle$ of ref. [35], used in our calculations, requires to calculate matrix elements of $\hat{j}_+$ between harmonic-oscillator basis states through a closure relation. In view of the truncation of the basis, we have checked the convergence of our calculated $\langle \hat{J}^2 \rangle$, even at the largest deformations involved, when using an "exact" formula, namely the expression (5) of ref. [35]. In the latter, only the sp states with $v_k^2 \neq 0$ are needed. It has been found, for both the first and the second fission barriers of ^{252}Cf, that the rotational correction energy differs by less than 1 keV. It is worth noting here that a renormalisation of the moment of inertia evaluated by the Belyaev formula is yielded by the time-odd density response to the time-odd mean field [36] dubbed in some previous papers [37] as the Thouless-Valatin corrective term. It amounts to about 30% with the Gogny D1S force, as it has been found some time ago in the Bruyères-le-Châtel works, and depends strongly on the effective force in use and more specifically on their effective mass. Indeed in a recent paper [38] it has been shown to be merely 20% for the SIII Skyrme force ($m^*/m = 0.76$) and 10% for the SkM* force ($m^*/m = 0.79$). It is worth mentioning here that such a dependence on the m^*/m ratio had been reported by M.J. Giannoni and one of the authors of the present paper (Ph. Q.) as far as quadrupole mass parameters are concerned [39]. In view of the rather rough character of the whole approach of this rotational correction, we have not found appropriate to overload the discussion with such a 10% effect on a corrective term.

In principle, one should make use of the Yoccoz moment of inertia [40]. However, we have limited ourselves to a simpler approximation. As mentioned above, we perform here an approximate projection assuming a rotational character for the projected good J states $|\Phi_J\rangle$. Furthermore, expanding the nucleus wave function $|\Psi\rangle$ onto the normalized $|\Phi_J\rangle$ states, we make the following hypothesis of rigid rotation for the energies [33,41,42]:

$$\langle \Phi_J | \hat{H} | \Phi_J \rangle = E_0 + \frac{J(J+1)\hbar^2}{2\,\mathcal{I}}\,, \tag{6}$$

where $\mathcal{I}$ is a moment of inertia. In the frame of the rigid-rotation assumption, $\mathcal{I}$ is constant with J. It may thus be evaluated, in particular, in the adiabatic limit of the Thouless-Valatin (Routhian) formalism. The latter gives, up to self-consistent time-odd terms in the Hartree-Fock and pairing fields, the Inglis-Belyaev moment of inertia. As discussed above, the contribution of the time-odd fields can be taken care of upon multiplying the Inglis-Belyaev moments by an appropriate factor depending on the effective force used.

Table 3. Energy differences ΔE (in MeV) between the ground state and the $Q_{20} = 65$ b point near the top of the axial first barrier of ^{252}Cf and Q_{22} corresponding values obtained with different $N_{\rm F}$-values.

$N_{\rm F}$	Q_{22} (fm^2)	ΔE
3	455	9.333
5	583	8.027
7	573	8.062
9	573	8.062
11	573	8.062

2.4 Triaxial calculations

In phenomenological studies of fission barriers [2,6] it has been shown that the first barrier of heavy nuclei is no longer axially symmetric. Thus, the first saddle point energy is lowered when allowing triaxial shapes for the nucleus undergoing fission —while left-right asymmetry is not favored at this point. This is why we have performed deformation energy calculations around the first saddle point using the reflection symmetrical triaxial HF + BCS code of ref. [22]. All the quantities depending on the azimutal angle involved in this code have been decomposed into Fourier series, leading to a truncated expansion. The maximum number of Fourier components, $N_{\rm F}$, has to be considered as a parameter on which physical quantities can spuriously depend, as is the case, *e.g.*, for N_0. We have checked that the quadrupole moment Q_{22} as well as the energy relative to the ground state are reasonably converged for $N_{\rm F} = 7$ (see table 3).

In order to obtain the lowest triaxial solution at a given Q_{20}-elongation, a section in the corresponding two-dimensional potential energy surface has first to be drawn. The seeked minimum can then be roughly localized and one can perform a final calculation starting from an approximate solution by releasing the constraint on Q_{22}. Triaxial solutions that have been obtained correspond to low γ-values ($\gamma \approx 15^\circ$ at most), so that they remain rather close to symmetrical ones. Therefore, assuming that the basis parameters used for triaxial calculations should be close to those obtained in the axial calculation corresponding to the same Q_{20}-value, we have decided to perform all triaxial calculations with the b- and q-values retained in the axial cases. This assumption has been checked to be roughly true at the top of the first (triaxial) fission barrier of ^{236}U and ^{252}Cf (see table 2).

2.5 Reflection asymmetric calculations

Most existing axial Skyrme-Hartree-Fock codes have considered only left-right symmetrical solutions, that is solutions having the equatorial plane (perpendicular to the symmetry axis) as a reflection symmetry plane. Consequently, the center of mass of the nucleus belongs in the symmetrical case, to this plane and corresponds to $z = 0$. In the intrinsic frame the parity symmetry is thus explicitly imposed. Now, phenomenological studies have predicted the lowering of the second barrier when allowing

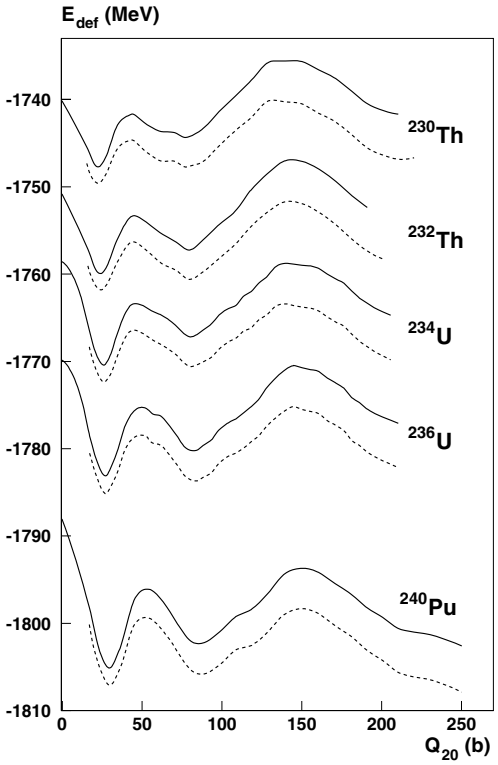

Fig. 3. Deformation energy curves of two Th isotopes, two U isotopes and one Pu isotope including rotational correction within the HF + BCS(G) approach. For each isotope, the dashed lines (full lines, respectively) correspond to calculations with (without, respectively) rotational energy correction.

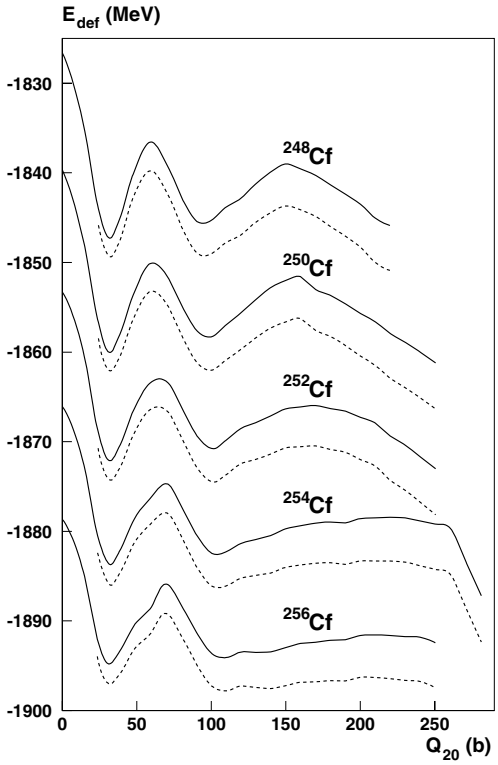

Fig. 4. Same as fig. 3 for five Cf isotopes.

left-right asymmetric shapes. We thus have extended our axial code so as to allow a breaking of the parity symmetry. To achieve this goal we have released the condition $f(r,z) = f(r,-z)$ for any function f involved in the symmetrical code and we have replaced the integrals of the form $2\int_0^{+\infty} f(r,z)\mathrm{d}z$ with $\int_{-\infty}^{+\infty} f(r,z)\mathrm{d}z$. This amounts to mix Ω^- and Ω^+ (with usual notations) submatrices in the Hartree-Fock Hamiltonian matrix to be diagonalized. We have also constrained the center-of-mass position to remain at the origin of the intrinsic frame. Due to the symmetries of our solutions, it is sufficient to impose that $\langle z \rangle = 0$.

In order to investigate the effect of parity breaking on the deformation energy curve in the vicinity of the second barrier, we have added a constraint on the axial octupole moment Q_{30} defined by

$$Q_{30} = \int \mathrm{d}^3\mathbf{r}\, \rho(\mathbf{r}) Y_3^0(\theta,\varphi) \tag{7}$$

with usual notations for the spherical harmonics $Y_\ell^m(\theta,\varphi)$ and where $\rho(\mathbf{r})$ is the nucleon density in coordinate space. The same procedure as the one described in sect. 2.4 has then been followed (with Q_{30} playing the same role as Q_{22} there) to find the fission path through the second saddle point. Moreover, we have assumed that the basis parameters b and q corresponding to the left-right symmetrical solution at a given Q_{20}-elongation remain optimal for the asymmetric solution at the same elongation. Indeed the latter solution is associated with a quite weak octupole moment (namely a few barns$^{3/2}$), at least up to the tops of both the symmetrical and asymmetrical second barriers. It has been checked for ^{236}U and ^{252}Cf (see table 2) that the height of the asymmetrical second barrier is not affected by the change of optimal basis parameters with increasing Q_{30}-values from zero.

3 Results

3.1 HF + BCS(G) calculations with rotational correction

Within the above-described HF + BCS(G) framework, we have calculated the deformation (potential) energy curves of twenty-six even-even nuclei, namely: two Thorium isotopes (^{230}Th and ^{232}Th), two Uranium isotopes (^{234}U and ^{236}U), the ^{240}Pu isotope, five Californium isotopes (from ^{248}Cf to ^{256}Cf), thirteen Fermium isotopes (from ^{240}Fm to ^{264}Fm) and three Nobelium isotopes (from ^{252}No to ^{256}No).

The results for solutions constrained to have axial and reflection symmetries are presented in figs. 3 to 6. They are also summarized in table 4, where three energies of relevance are reported (when available): the heights of the

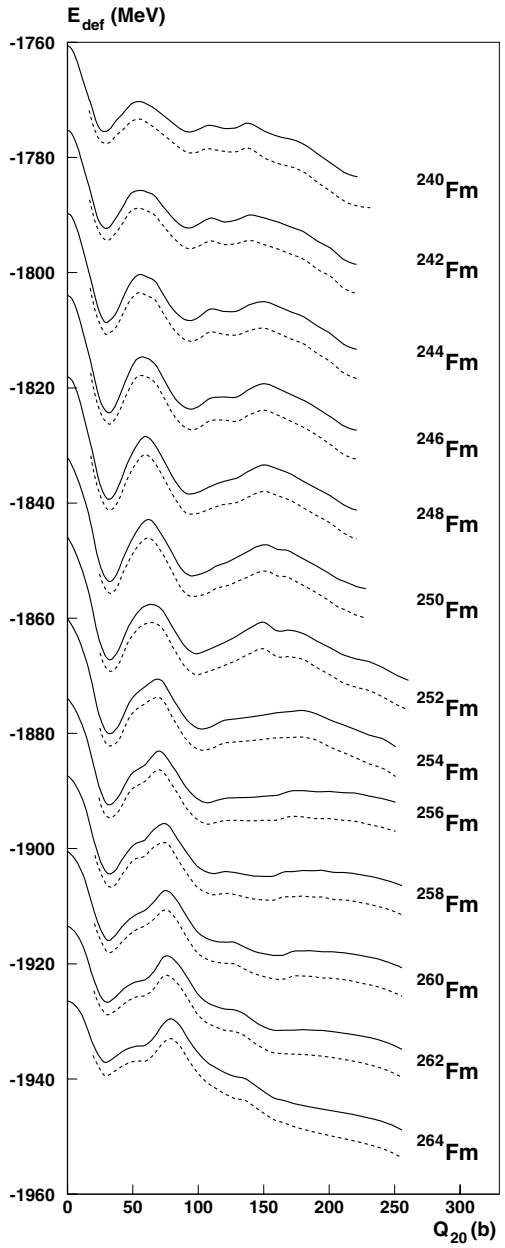

Fig. 5. Same as fig. 3 for thirteen Fm isotopes.

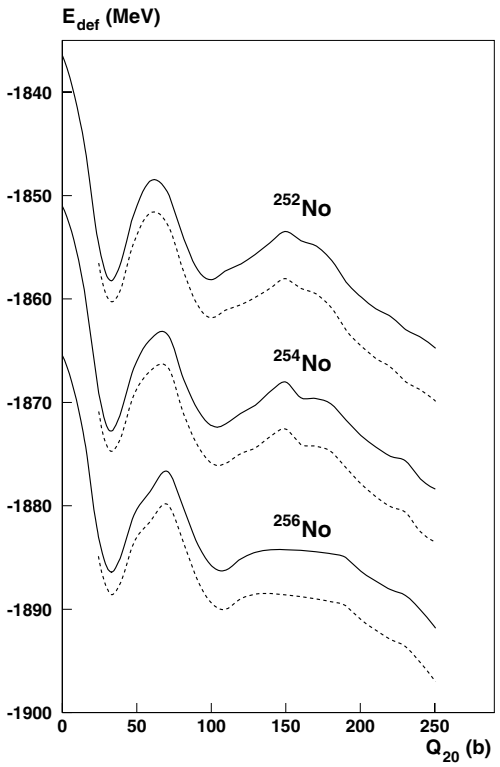

Fig. 6. Same as fig. 3 for three No isotopes.

first (E_A) and the second (E_B) fission barriers together with the excitation energies ($E_{\rm II}$) of the fission super–deformed (SD) isomers. In all cases, the corresponding total energies are relative to the normal deformed (ND) local equilibrium solutions.

Let us first discuss the results obtained *without* the inclusion of the rotational correction. Considering the lowest-energy solution as a function of the quadrupole moment as the ground-state (gs) configuration, one notes that the gs shapes always correspond to ND configurations, which means that the isomeric energy $E_{\rm II}$ is positive —except for the ^{240}Fm isotope. The first fission barrier height E_A does not vary very much for all calculated nuclei (remaining in the 6–10 MeV range). On the contrary, E_B exhibits a rather strong variation upon increasing A. For the five lighter calculated (Thorium, Uranium and Plutonium) isotopes, the first fission barrier is smaller than the second one ($E_A < E_B$). One obtains just the opposite for all other calculated isotopes.

We now proceed to present the results of our axial calculations upon including the above-discussed rotational correction (see sect. 2.3). In fig. 7 (fig. 8, respectively) we have plotted the curves of $\langle \hat{J}^2 \rangle$ (respectively $\mathcal{I}_{\rm Bel}$) as functions of the mass quadrupole moment Q_{20} for five Californium isotopes as typical examples. In all isotopes they are on the whole both increasing functions of the deformation. However, the resulting corrective term (proportional to the ratio of $\langle \hat{J}^2 \rangle$ and $\mathcal{I}_{\rm Bel}$) is, as already noted [10], an increasing function of the elongation for large enough Q_{20}-values (namely near the ND deformations and beyond), as can be seen in fig. 9 in the case of ^{252}Cf taken as example. This is due to the fact that, there, the former varies with a power of Q_{20} which is larger than for the latter, as seen in figs. 7 and 8. This should not be so clear for small deformations where, anyway, the rotational spectrum approximation for the projected energies is by no means a relevant approximation. This is why, in figs. 3 to 6, the corrected potential energy curves (corresponding to the dashed curves) are plotted only for deformations around and beyond the ND solutions.

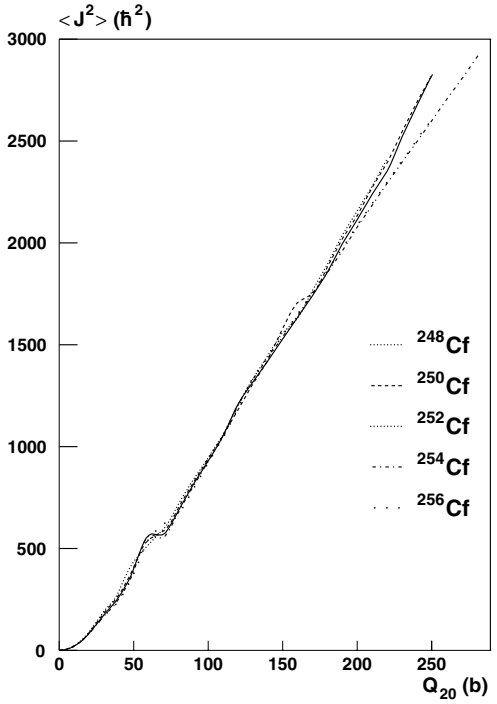

Fig. 7. Expectation value $\langle \hat{J}^2 \rangle$ (in $\hbar^2$ units) as a function of Q_{20} (in barns) within the HF + BCS(G) approach for five Cf isotopes.

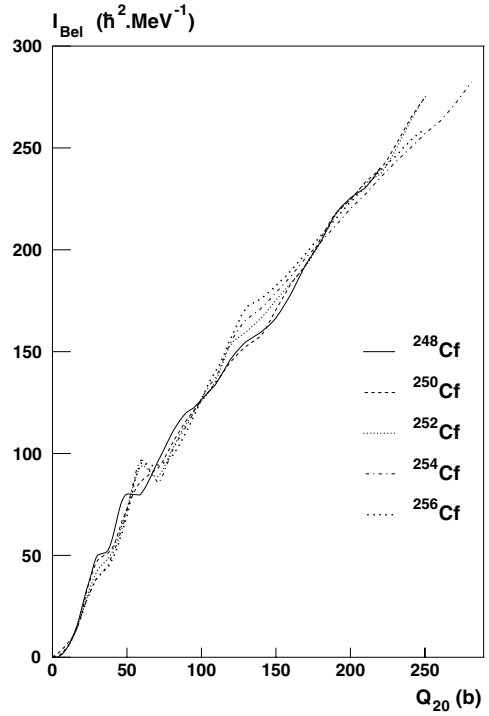

Fig. 8. Belyaev moment of inertia (in $\hbar^2 \mathrm{MeV}^{-1}$ units) as a function of Q_{20} (in barns) within the HF + BCS(G) approach for five Cf isotopes.

Table 4. HF + BCS(G) relative energies (in MeV) of the first barrier, of the superdeformed minimum and of the second barrier with respect to the energy of the normally deformed minimum for the twenty-six calculated nuclei. They are evaluated without and with rotational correction. No values of E_{II} and E_B are given for Fm isotopes heavier than ^{256}Fm and for ^{240}Fm, since the fission barriers of these nuclei are single-humped.

	E_A		E_{II}		E_B	
Nucleus	without	with	without	with	without	with
^{230}Th	6.0	4.9	3.3	1.8	12.1	9.3
^{232}Th	6.5	5.5	2.7	1.2	12.9	10.0
^{234}U	6.8	5.8	3.2	1.8	11.7	9.0
^{236}U	7.9	6.7	2.9	1.5	12.6	10.0
^{240}Pu	9.0	7.6	2.8	1.3	11.4	8.8
^{248}Cf	10.7	9.6	2.0	0.1	8.3	5.7
^{250}Cf	10.3	9.2	1.7	0.1	8.5	5.8
^{252}Cf	10.1	9.1	1.3	−0.3	6.0	3.7
^{254}Cf	9.0	8.0	1.2	−0.3	5.2	2.6
^{256}Cf	8.9	7.9	0.7	−0.8	3.2	0.7
^{240}Fm	5.2	4.2	−0.1		1.4	
^{242}Fm	6.6	5.6	0.1	−1.4	2.3	0.0
^{244}Fm	8.3	7.2	0.3	−1.2	3.6	1.0
^{246}Fm	9.4	8.1	0.6	−1.0	5.1	2.4
^{248}Fm	10.9	9.6	0.9	−0.7	6.0	3.3
^{250}Fm	10.8	9.6	1.1	−0.1	6.4	3.8
^{252}Fm	9.2	8.1	1.1	−0.6	6.5	3.9
^{254}Fm	9.3	8.2	0.8	−0.7	4.0	1.5
^{256}Fm	9.3	8.3	0.3	−1.1	2.5	0.1
^{258}Fm	8.6	7.5				
^{260}Fm	8.7	7.4				
^{262}Fm	7.8	6.7				
^{264}Fm	7.6	6.5				
^{252}No	9.6	8.6	0.1	−1.5	4.8	2.2
^{254}No	9.6	8.6	0.4	−1.4	4.7	2.2
^{256}No	9.7	8.7	0.1	−1.5	2.2	0.1

The corrected values of the energies E_A, E_{II} and E_B are also reported in table 4. In view of the preceding discussion of the deformation dependence of the rotational correction, it is clear that they are always lower than their un-corrected counterparts. This entails, in particular, that the calculated Californium (with $A \geqslant 252$), Fermium and Nobelium isotopes have SD solutions which are lower in energy than the ND ones, by up to about 1.5 MeV for the heaviest isotopes. This result would mean that the ND minimum becomes an isomeric state as compared to the SD one which is therefore interpreted as the ground state. In our study it is the case for Fm isotopes heavier than $A = 242$ and for all other nuclei with $A \geqslant 252$. This result need not be inconsistent with the observation, for example, of ^{254}No through a γ cascade within its ND rotational band. Indeed, it has been experimentally obtained, *e.g.*, by Reiter *et al.* [43] as an evaporation residue of the ^{208}Pb(^{48}Ca, 2n) reaction with an excitation energy roughly equal to 8 MeV. That is much higher than the energy difference between the top of the second barrier

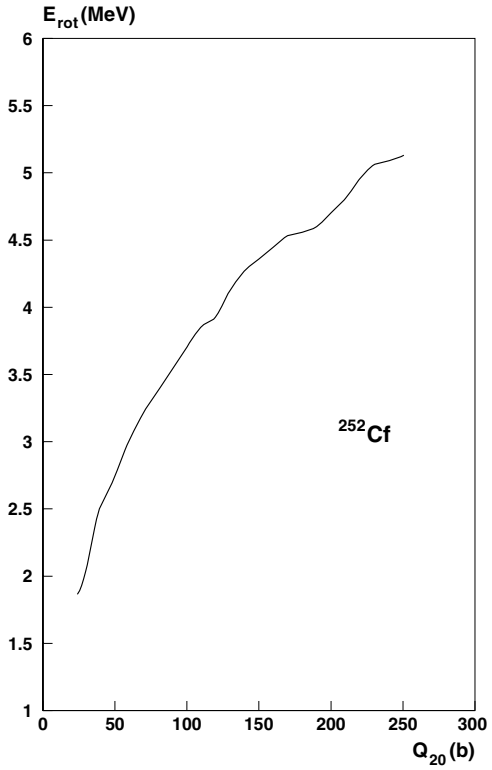

Fig. 9. Corrective energy of the zero-point rotational motion within the HF + BCS(G) approach for the ^{252}Cf isotope.

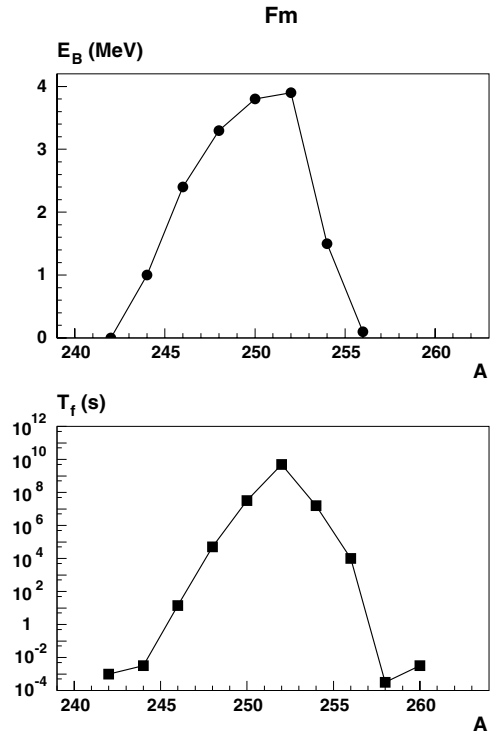

Fig. 10. Theoretical symmetric second-barrier heights (in MeV) including rotational correction (upper panel) and experimental fission half-lives (in s) of even Fm isotopes (lower panel). The experimental data are taken from ref. [47].

and the SD minimum ($E_B - E_{\rm II} = 3.6\,$MeV), so it would be difficult to observe the γ cascade of the evaporation-residue in the SD well due to a competition with the much favored spontaneous fission decay process. Since in our calculations $E_A = 8.6\,$MeV (when imposing axial symmetry though), the ND isomeric state seems less subject to this instability. This isotope has also been dealt with in theoretical works, in particular by the Madrid group who has performed Hartree-Fock-Bogoliubov calculations of the fission barriers at various spins with the Gogny D1S effective force [44] as well as by Duguet *et al.* with the Skyrme Sly4 force for the mean field and a density-dependant δ force for the pairing (adding the Lipkin-Nogami scheme to restore approximately the particle number) [45] and the Bordeaux group using the Skyrme SkM* interaction in the particle-hole channel and a seniority force in the particle-particle channel [46].

We now turn to the discussion of a striking feature of the evolution of the reflection-symmetric second barriers of the Fermium isotopes as functions of the mass A. It can be seen in table 4, in fig. 5 and especially in fig. 10, where the isomeric evolution of E_B as a function of A is reported (upper panel). The corrected barrier height increases from zero for $A = 242$ to 3.9 MeV for $A = 252$ and then drops with an increasing value of A. It almost vanishes for $A = 256$ ($E_B = 0.1\,$MeV), corresponding to a flat reflection-symmetric deformation energy curve beyond $Q_{20} = 100$ b. For higher neutron numbers, the double-hump pattern disappears into a single barrier. Beyond the top of this barrier, the deformation energy keeps a negative slope when Q_{20} increases, dropping all the more steeply as A increases. It is interesting to note that the above-discussed trend of E_B may be somewhat related to the experimental fission half-life pattern of even Fermium isotopes [47] (see the lower panel in fig. 10). Namely, the maximal value of T_f observed for ^{252}Fm can be explained by the maximal value of E_B for the same isotope. Moreover, up to a change from ^{256}Fm to ^{258}Fm, whenever E_B is almost vanishing the fission half-life turns out to be rather constant with A and relatively very short. In spite of the crude character of the calculations leading to that alleged relation between E_B and T_f, it should be stressed that it implies more than a possible coincidence, since it involves the location of three points in the half-lives curve (the starting points of the "bump" and its maximum) as well as the stationary character of the half-lives in cases where no second fission barrier is found. Quite on the contrary, we could be prone to think that precisely because our calculations do not imply all the effects that are discussed separately in the followig sections, the absence of fission barrier is very likely to be the main factor in the observed behaviour of the half-lives. Incidentally, one of the requested sophistications, namely to allow for asymmetrical fission, is bound to lower, if anything, the fission barrier, which would not infirm the statement on the

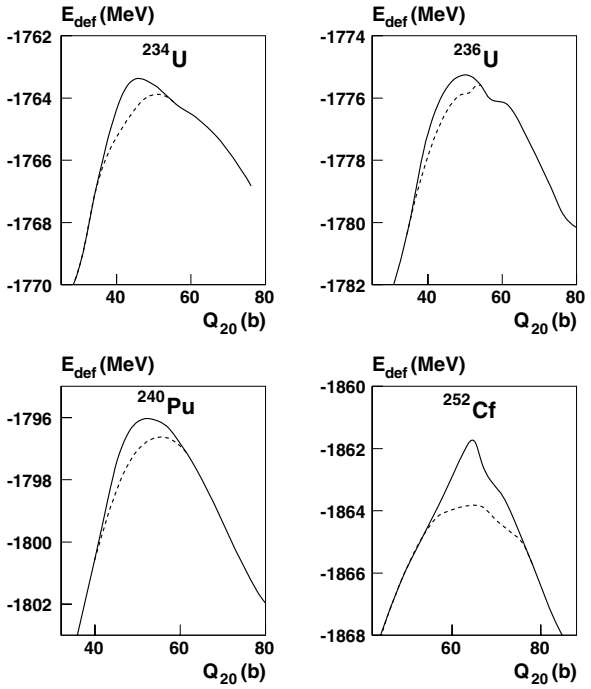

Fig. 11. First barrier of ^{234}U, ^{236}U, ^{240}Pu and ^{252}Cf within HF + BCS(G) approach (without rotational correction). The axial (respectively, triaxial) energies are plotted as full (respectively, dashed) lines.

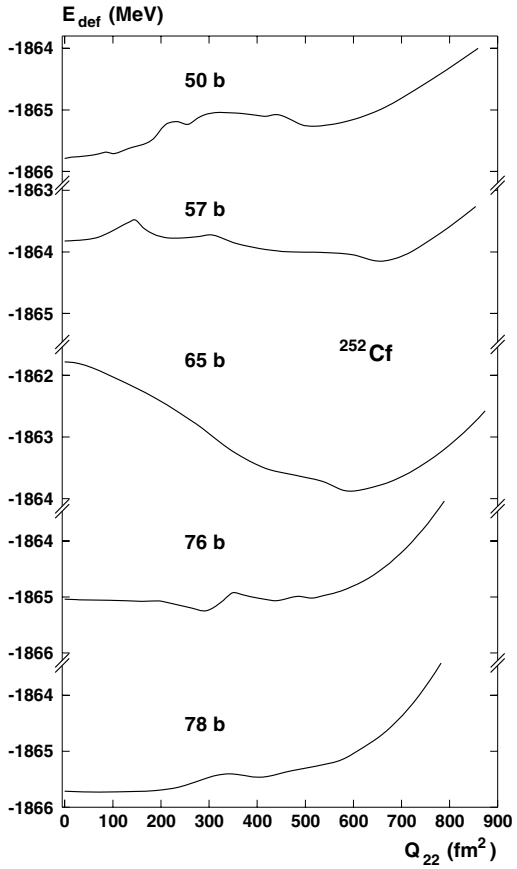

Fig. 12. Sections of the energy surface of ^{252}Cf as a function of Q_{22} (in fm^2) at different Q_{20}-elongations around the top of the first barrier. From top to bottom, the different curves correspond to increasing values of Q_{20}. They are plotted with the same scale.

absence of barrier but could modify the range of A-values where a second fission barrier exists.

At this point, we will not yet compare the calculated fission barrier heights with the experimental data when available, because it is well known that they should be lowered from their present values by allowing for triaxial shapes around the first fission barrier and for reflection asymmetric shapes around the second fission barrier. Such comparisons will thus be made in the two sections below where the results of calculations in which these symmetries have no more been imposed will be presented.

3.2 Triaxial calculations around the first fission barrier

The influence of triaxial deformations on the height of the first fission barrier has been investigated for four nuclei out of the 26 already mentioned (namely for the ^{234}U, ^{236}U, ^{240}Pu and ^{252}Cf nuclei). From the ND minimum up to the SD one, we have performed calculations allowing the nuclei to explore triaxial shapes. This additional degree of freedom leads, as expected, to new deformation energy curves lower than the axial ones (see fig. 11). It has been carefully checked that for each nucleus, one experiences a smooth transition from an axial to a triaxial shape in the vicinity of the top of the first barrier. While the effect on E_A is small in the three lighter calculated isotopes ($\Delta E_A \sim 0.5\,\mathrm{MeV}$), it is stronger for ^{252}Cf ($\Delta E_A \sim 2\,\mathrm{MeV}$).

The occurence of such a symmetry breaking is illustrated in the particular case of ^{252}Cf in fig. 12, where we have represented five sections of the potential energy surface along the Q_{22}-direction at different Q_{20}-elongations around the top of the first barrier. Indeed the Q_{22}-value of the energetically favored solution vanishes for the upper and lower curves and reaches its highest value for $Q_{20} \approx 65$ b. This deformation also turns out to be approximately the deformation of the barrier top for an axial solution (this is also the case for the three other nuclei considered in this section). It is associated with the maximal energy difference between axial and non-axial solutions as can be seen in fig. 11. The $Q_{20} = 65$ b section of the energy surface in fig. 12 shows that the energy difference associated with the symmetry breaking amounts to roughly 2 MeV, as already mentioned, corresponding thus to a triaxial E_A-value of 8.1 MeV (see table 4).

As mentioned in sect. 2.3, the rotational correction has not been explicitly computed in the triaxial case. To take it approximately into account, we have substracted to the triaxial energy the rotational energy calculated in the axial case at the same Q_{20}-value. As we have seen, the position

Table 5. Experimental —when available— and theoretical (HF + BCS(G) + rotational correction) barrier heights and isomeric state energies (in MeV) of six heavy nuclei. Experimental data are taken from [15], except for ^{252}Cf [17] and for the $E_{\rm II}$-value of ^{232}Th [48]. The hyperdeformed minimum relative energy $E_{\rm III}$ and the third barrier height E_C of Thorium isotopes are compared with the results of Berger *et al.* [12]. The values appearing with an asterisk correspond to axial solutions.

	E_A		$E_{\rm II}$		E_B		$E_{\rm III}$		E_C	
Nucleus	exp.	this work	exp.	this work	exp.	this work	[12]	this work	[12]	this work
^{230}Th	6.1	4.9*		1.8	6.5	4.4	5.0	3.2	5.7	3.6
^{232}Th	5.8	5.5*	2.8	1.2	6.2	4.1	4.2	2.7	4.3	3.0
^{234}U	5.6	5.3		1.8	5.5	5.1				
^{236}U	5.6	6.2	2.3	1.5	5.6	4.6				
^{240}Pu	5.6	7.1	2.4	1.3	5.1	4.1				
^{252}Cf	5.3	7.1		−0.3	3.5	2.9				

of the triaxial top of the barrier is the same as what has been obtained for the axial one. Moreover, the rotational correction does not significantly shift the fission barrier deformation. Consequently, since the ND minimum corresponds to an axial solution, the triaxial barrier height with rotational correction can thus easily be evaluated as the difference between the energies of the ND corrected minimum and the (approximate) so-corrected triaxial energy at the fission barrier top.

Table 5 displays the theoretical values of E_A obtained as above indicated, together with the experimental data taken from refs. [15, 17, 48]. The agreement is seen to be rather good for the two considered Uranium isotopes (within 0.6 MeV). Our estimates for the ^{240}Pu and the ^{252}Cf isotopes are too large by 1.3 and 1.8 MeV, respectively. For the former, our result is slightly better, though, than what has been obtained in the HFB calculations of ref. [12].

3.3 Reflection asymmetric calculations around the second fission barrier

The influence of the parity breaking on the second fission barrier height has been investigated for the four nuclei considered in the previous section and the two ^{230,232}Th isotopes. From the SD minimum up to far beyond the second saddle point, we have performed calculations allowing the nuclei to explore left-right asymmetrical shapes. Namely, starting from a reflection-symmetric solution at a given value of Q_{20}, we have searched for an equilibrium solution with a non-vanishing Q_{30} for the same Q_{20}. In doing so, we have found in all cases that the Q_{40}-values, with the following definition:

$$Q_{40} = \int \mathrm{d}^3\mathbf{r}\, \rho(\mathbf{r}) Y_4^0(\theta, \varphi), \tag{8}$$

were not varying violently (typically less than 10%), except for the ^{252}Cf nucleus, where it reaches 40% at $Q_{20} =$ 150 b and otherwise decreases to values smaller than 10% (see fig. 13). Upon plotting both reflection-symmetric and non-symmetric curves as a function of Q_{20}, we have found that the deformation energy curve is lowered in the latter case (see further, figs. 14 to 17). For all studied nuclei the deformation energy curves associated with asymmetrical solutions exhibit the same characteristic pattern.

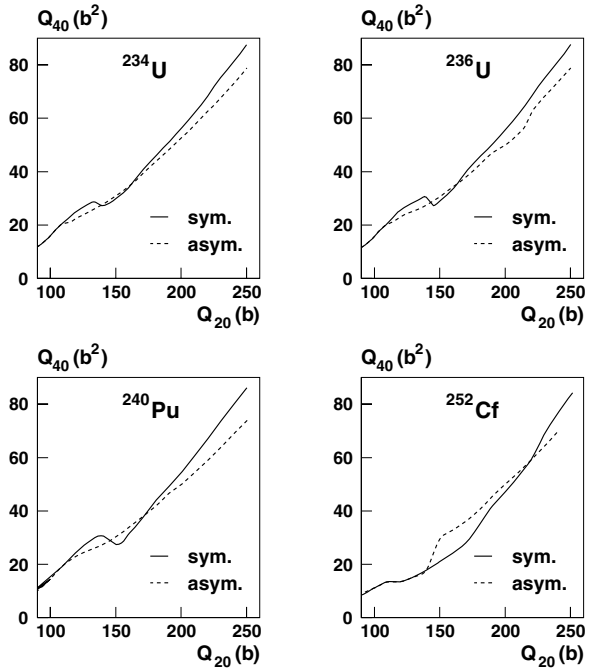

Fig. 13. Q_{40}-values (in barns^2) as functions of Q_{20} (in barns) corresponding to asymmetrical calculations compared with those corresponding to symmetrical ones for ^{234}U, ^{236}U, ^{240}Pu and ^{252}Cf.

Namely, from the SD minimum up to a particular "branching point" —whose abscissa depends on the considered nucleus— the left-right symmetrical shape is energetically favored. Then, from this branching point up to far beyond the second saddle point, the most stable solution becomes the asymmetric one. Furthermore, the branching point almost coincides with the top of the second asymmetric barrier, making the symmetric-asymmetric transition rather sudden.

To illustrate in a more detailed fashion one of these transitions, we have studied the particular example of ^{252}Cf. We have performed calculations in which both Q_{20} and Q_{30} have been constrained so as to obtain sections of the potential energy surface along the Q_{30}-direction at different elongations. The corresponding results are shown in

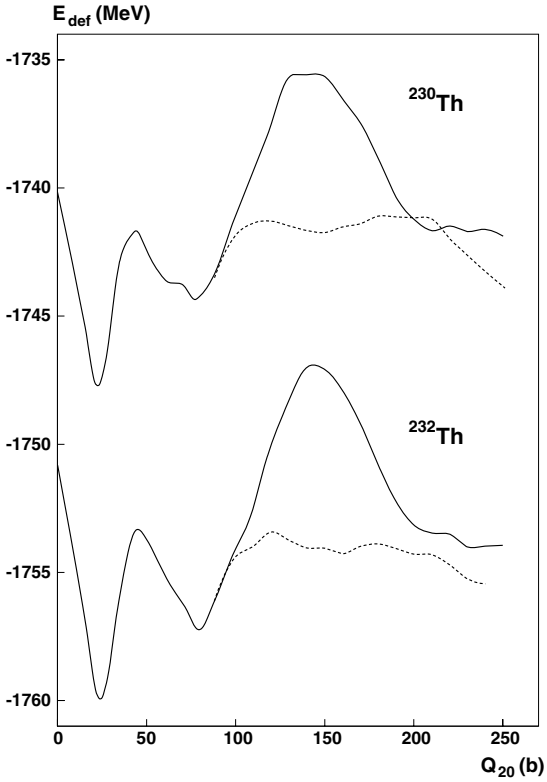

Fig. 14. Deformation energy curves (without rotational correction) of ^{230}Th and ^{232}Th within HF + BCS(G) approach. The reflection asymmetric effect is shown with dashed lines.

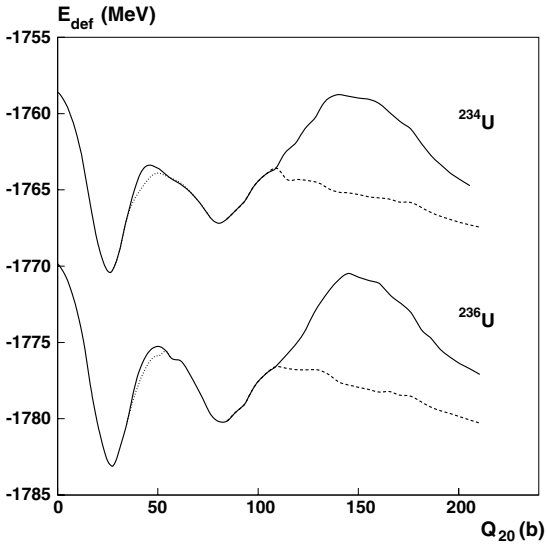

Fig. 15. Deformation energy curves (without rotational correction) of ^{234}U and ^{236}U within HF + BCS(G) approach. The triaxial and reflection asymmetric effects are shown with dotted and dashed lines, respectively.

fig. 18. The curve corresponding to $Q_{20} = 130$ b presents a single well-pronounced minimum for symmetric shape

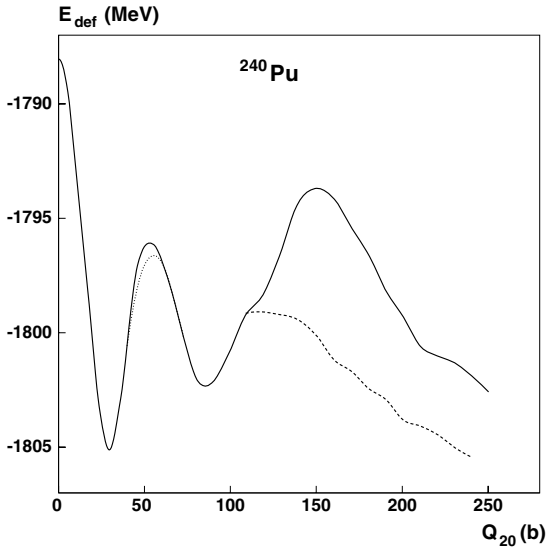

Fig. 16. Same as fig. 15 for the ^{240}Pu isotope.

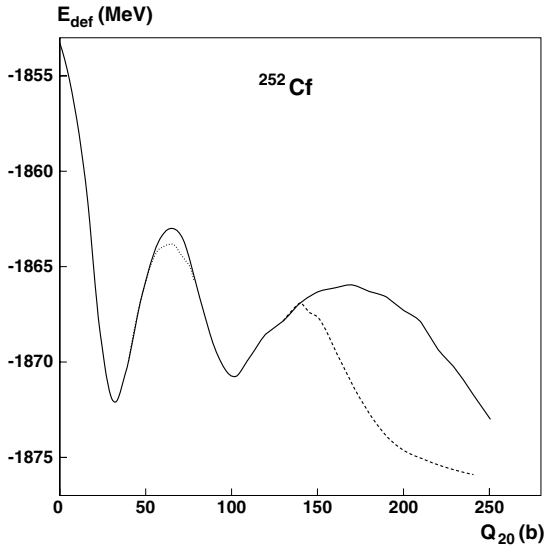

Fig. 17. Same as fig. 15 for the ^{252}Cf isotope.

($Q_{30} = 0$), whereas at higher Q_{20}, a second local minimum appears at finite Q_{30}. Then, increasing Q_{20} the first minimum becomes less marked and even vanishes above $Q_{20} = 140$ b, while the second one appears to be energetically favored. The transition between the two valleys does not proceed through a tunneling between two "crossing" valleys but rather the barrier between them is progressively diminishing to totally disappear when the two local minima are almost degenerate.

In the upper part of fig. 18, we represent the variation of Q_{30} associated with the lowest energy solution as a function of Q_{20}. The obtained pattern is reminiscent of a first-order phase transition where the order parameter would be Q_{30}. Within this picture, the critical value of the elongation is $Q_{20}^{c} = 140$ b.

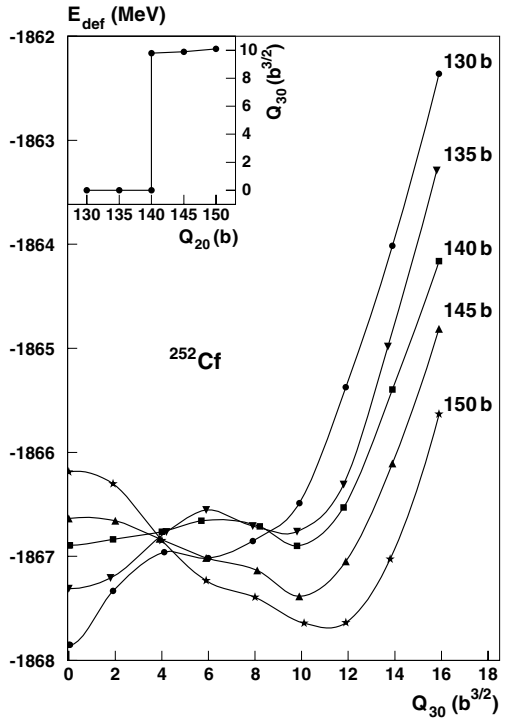

Fig. 18. Sections of the deformation energy surface as functions of the octupole moment Q_{30} (in barns$^{3/2}$) for ^{252}Cf at different elongations around the top of the second barrier.

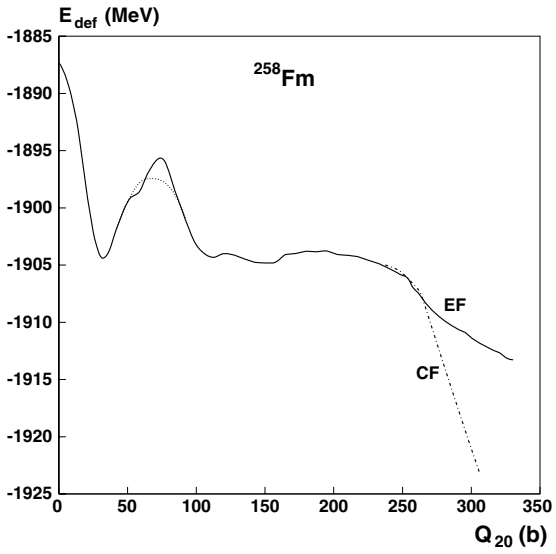

Fig. 19. Same as fig. 15 for the ^{258}Fm isotope. The dash-dotted line represents the "compact" fission path, whereas the full line corresponds to the "elongated" one.

As for the shape of the second barriers, it appears to be drastically modified by taking into account this additional degree of freedom. Namely, the barrier height is lowered by about 1 MeV in ^{252}Cf up to almost 6 MeV for ^{236}U, and the barrier width is considerably quenched, the more so for ^{252}Cf. This clearly indicates that a relevant fission half-life calculation should, of course, take into account this symmetry breaking. It should be noticed that the asymmetrical deformation energy curves of both studied Thorium isotopes exhibit a third well, corresponding to a ternary hyperdeformed (HD) minimum. This well has been experimentally seen (see, *e.g.*, [49]) but is found rather shallow in our calculations. This feature has been already obtained in the Hartree-Fock-Bogoliubov calculations of Berger *et al.* [12] using the D1S effective interaction both in the particle-hole and the particle-particle channels. In particular, they have predicted that the HD well is deeper for ^{230}Th than for ^{232}Th. As can be seen in table 5, presenting the energies of the ternary minimum $E_{\rm III}$ and of the third fission barrier E_C relative to the ND minimum, our calculations confirm this prediction, since the depths of the HD well in both isotopes, *i.e.* the values of $E_C - E_{\rm III}$, are of the same order of magnitude in both calculations —a few hundred keV— and since we have also found the third well deeper in ^{230}Th than in ^{232}Th.

In table 5 we compare also the experimental and theoretical second-barrier heights (allowing for reflection asymmetric shapes) of the six nuclei under study here. The rotational correction has been included in a way which is similar to what has been sketched in sect. 3.1. For the ^{234}U, ^{236}U and ^{240}Pu nuclei, only left-right symmetry breaking allows to obtain, as found experimentally, a second-barrier height E_B comparable to or lower than the first one. Beyond this qualitative agreement, it should be stressed that the difference between experimental and theoretical E_B-values is found to be of the order of 1 MeV, which is quite encouraging.

To end up with the discussion of the effect of breaking some geometrical symmetries, we have performed calculations, without rotational correction, along two different fission paths in ^{258}Fm —known to experience bimodal fission— upon letting the nucleus free to explore reflection asymmetrical shapes beyond the SD minimum as can be seen in fig. 19. The dash-dotted line represents the "compact" fission path whereas the full line corresponds to the "elongated" one, as dubbed by Warda *et al.* Along both paths the fissioning nucleus turns out to keep preferably a symmetrical shape owing to the proximity of twice the doubly magic ^{132}Sn nucleus. This does not eliminate the possibility of an even more complicated topology of the potential energy surface in the descent from the saddles to the scission points (as some preliminary calculations, which are beyond the scope of this paper dealing with fission barriers, tend to show). But the important point here is to strongly insist on the fact that the existence of both a compact and an elongated path (which are thought in the vicinity of the second saddle the most relevant) do not influence in this particular case the second-fission-barrier height. We have also included the γ degree of freedom around the first fission barrier (dotted line) and found a lowering of roughly 2 MeV.

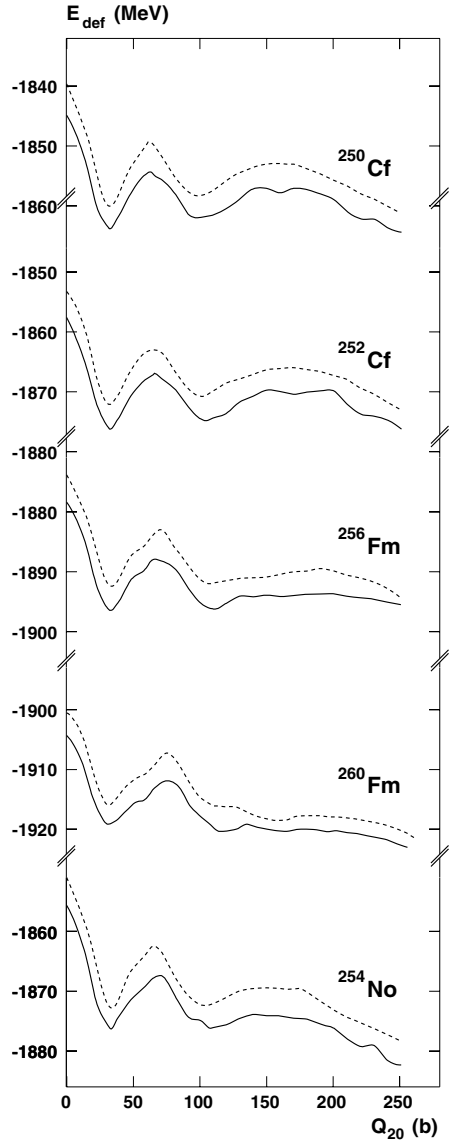

Fig. 20. Comparison of the deformation energy curves of five nuclei within HF + BCS(G) (dashed line) and HF + BCS(δ) (full line) approaches (without rotational correction).

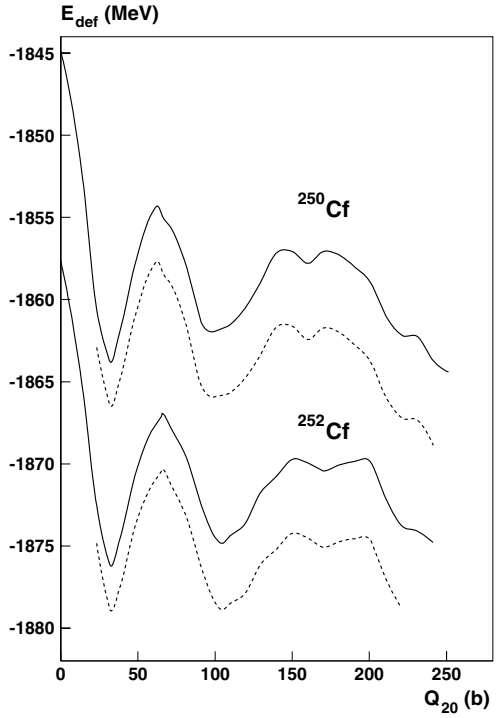

Fig. 21. Deformation energy curves of two Cf isotopes including rotational correction within the HF + BCS(δ) approach. For each isotope, the dashed line (full line, respectively) corresponds to calculations with (without, respectively) rotational energy correction.

3.4 HF + BCS(δ) calculations

We have also performed HF + BCS calculations with a residual δ-interaction for five nuclei among those considered in sect. 3.1, namely ^{250,252}Cf, ^{256,260}Fm, and ^{254}No. At first we have compared the results of HF + BCS(δ) and HF + BCS(G) calculations in fig. 20 which displays in both cases the deformation energy curves without rotational correction. Both patterns appear clearly to be very similar. In particular, the gs shapes still correspond to ND configurations and the corresponding Q_{20}-values are very close to those obtained within HF + BCS(G) approach (to within 1 b). The latter remark can be somewhat extended to the SD minima, since corresponding Q_{20}-values are similar to those yielded by HF + BCS(G) calculations within less than 5 b. Moreover, the HF + BCS(δ) calculations yield a low E_B-value in ^{256}Fm and predict the disappearance of the second barrier in ^{260}Fm. This is also what has been obtained within HF+BCS(G) calculations. Nevertheless, it should be noticed that the detailed pattern of the HF + BCS(δ) curves is less regular. This is especially so for the two calculated Californium isotopes. Indeed, it can be seen on the full line curves of fig. 21 (with a scale different from the one of fig. 20) that the top of the reflection-symmetrical second barrier exhibits a ternary minimum, with a well depth that does not exceed 750 keV. This arises from structural effects of the pairing δ-force. Taking the example of ^{250}Cf —for which the latter is the most significant— the bottom of the well lies at 160 b, where the sp spectra show two phenomena. On the one hand, three neutrons states turn out to be almost degenerate at the Fermi level, leading to particularly strong neutron pairing correlations. On the other hand, the proton pairing energy undergoes a sudden 4.5 MeV decrease between 150 b and 160 b, and then its variation does not exceed 0.3 MeV up to 180 b. Both phenomena appear clearly in fig. 22 when looking at the curves representing neutron and proton pairing energies (referred to as E_n and E_p, respectively) as functions of the elongation. They lead to a local minimum in the total pairing

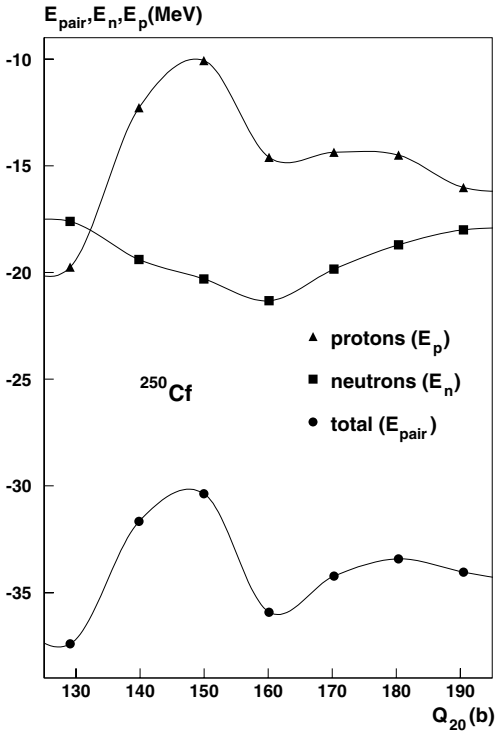

Fig. 22. Neutrons, protons and total pairing energies obtained within the HF + BCS(δ) approach around the second fission barrier of ^{250}Cf.

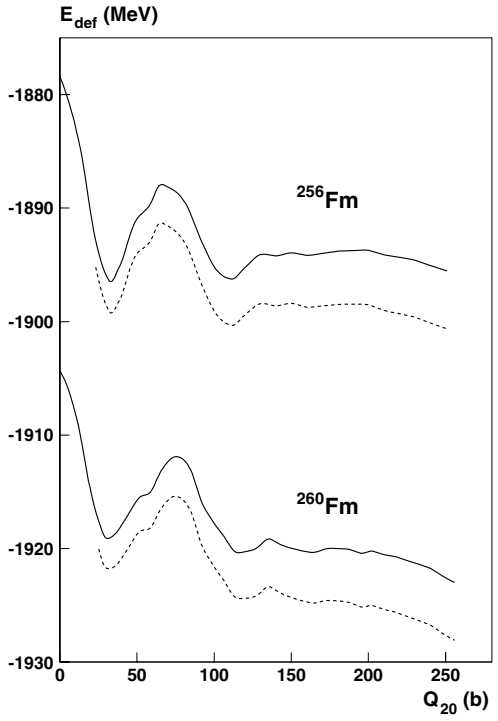

Fig. 23. Same as fig. 21 for two Fm isotopes.

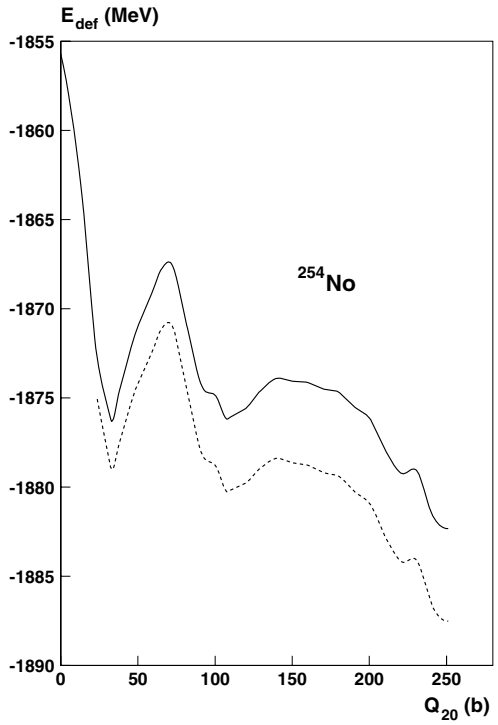

Fig. 24. Same as fig. 21 for ^{254}No.

energy ($E_{\rm pair}$) curve, as shown in fig. 22, where it has been represented together with E_n and E_p.

We have also performed calculations including the rotational correction discussed in sect. 3.1. The corresponding results are displayed in figs. 21, 23 and 24, which are the HF + BCS(δ) counterparts of figs. 4 to 6 restricted to the above-listed five nuclei. It can be seen that the rotational correction produces the same effects as described in sect. 3.1. The HF + BCS(δ) barrier heights and the isomeric energies, without and with correction, are reported in table 6, together with those deduced from the HF + BCS(G) calculations. Looking at the corrected values, it appears that the barrier heights obtained with both pairing forces differ by less than 1 MeV, except for the E_B-value in ^{254}No with a difference amounting to 1.7 MeV. These two *a priori* rather different pairing interactions yield the same fission barriers. It is likely therefore that they provide a good description of the fission process (at least up to the second saddle point).

To end this discussion, a word of caution is worth adding here. One should be careful when comparing the binding energies provided by approaches in which the mean field and the pairing are treated with different interactions. Indeed using, for example, a Skyrme plus a seniority or delta interaction in the pairing channel is anything but inconsistent as opposed to the case of the Gogny force. This has the effect that one cannot define reasonably a correlation energy because it would involve a comparison between two expectation values with different Hamiltonians.

Table 6. HF + BCS(G) and HF + BCS(δ) relative energies (in MeV) of the first barrier, of the superdeformed minimum and of the second barrier with respect to the energy of the normally deformed minimum for five nuclei. They are evaluated without and with rotational correction. For each nucleus, the first line corresponds to BCS(G) calculations and the second one to BCS(δ) calculations.

	E_A		$E_{\rm II}$		E_B	
Nucleus	without	with	without	with	without	with
	10.3	9.2	1.7	0.1	8.5	5.8
^{250}Cf	9.4	8.7	1.8	0.5	6.7	4.8
	10.1	9.1	1.3	−0.3	6.0	3.7
^{252}Cf	9.2	8.5	1.3	0.0	6.4	4.6
	9.3	8.3	0.3	−1.1	2.5	0.1
^{256}Fm	8.4	7.7	0.2	−1.2	2.7	0.6
	8.7	7.4				
^{260}Fm	7.2	6.4				
	9.6	8.6	0.4	−1.4	4.7	2.2
^{254}No	8.5	7.8	0.1	−1.3	2.3	0.5

4 Conclusions and perspectives

The present paper aimed at assessing the capability of state-of-the-art microscopic approaches to perform numerically sound and physically relevant calculations beyond the second fission barrier in actinide and heavier nuclei.

To match this purpose, we have first addressed thoroughly some important technical questions. In such static calculations using the Skyrme effective interaction and where the HF sp states are expanded onto some harmonic-oscillator basis, one generally evaluates some local densities and computes some relevant matrix elements through a discrete mesh corresponding to the zeros of the orthogonal polynomials associated with a Gauss integration method (Gauss-Hermite in the fission axis direction, Gauss-Laguerre in the perpendicular plane). In this respect, the stability of the results in terms of the number of considered mesh points has been validated, especially for the very large elongations encountered at the end of the fission process. This study has been extended to the symmetry breaking situations experienced near the barriers (triaxial shapes around the first barrier and intrinsic parity breaking shapes near the second one). On the other hand, the treatment of pairing correlations has also been checked. It has been made use of two simple versions of a consistent (up to a certain point) BCS treatment (namely using the so-called seniority and density-independent delta forces, respectively). As well known, in such a non-convergent approximation, the global pairing strength has to be fixed according to a given sp configuration space in which one allows for pair diffusion. We have chosen the intensity (the same for all calculations) for both forces, so that the amount of pairing correlations in some nuclei at, *e.g.*, their equilibrium intrinsic deformations, should be roughly the same in both cases. One has then shown here that the deformation dependence of these correlations, and correlatively the potential energy curves which they produce, seems rather independent of the details of the matrix element of the residual interaction. The rotational energy content of our deformed intrinsic states varies almost regularly and significantly with the elongation. We have demonstrated here that such an energy correction (evaluated within a very crude estimate able, however, to yield the trend of its deformation dependence) was also fully converged. However, fission barrier calculations with angular-momentum projection performed recently by P.-H. Heenen [50] seem to indicate that our energy correction has been overestimated, which means that our fission barriers have been underestimated. But it should be kept in mind that, even though the parity symmetry breaking (in the vicinity of the second saddle point) has led to solutions of lower energies, the latter do not correspond to states of good parity. Upon projecting on positive-parity states, one would obtain an extra corrective term which would lower the barrier, as showed by Bonche *et al.* in a similar study [51]. Our results are therefore likely to be modified in a way depending directly on the difference between the effects of the two above-mentioned projections on the relative energy around the second fission barrier, which is a still unknown quantity.

Let us now turn to the output of our approach. In view of the global agreement of our fission barriers with currently retained estimates from experimental data (for fission at very low energy), we may first conclude that the SkM* Skyrme interaction combined with a reasonable pairing strength estimate, constitutes a rather good choice for the effective nucleon-nucleon interaction. A better treatment of pairing correlations in the considered even-even nuclei would be advisable, particularly in cases where one experiences gaps near the Fermi surface in the sp spectrum. This would absolutely be necessary for a fair description of the fission barriers of odd or odd-odd nuclei, particularly in what concerns the so-called specialisation energy. Such calculations are currently under way. As for the zero-point motion energies, we have only considered here the rotational mode and not, for instance, the two independent quadrupole vibrational modes as done in, *e.g.*, ref. [12]. The reason is that for the former a clean-cut almost continuous elongation dependence (whose good reproduction is of course requested for the evaluation of a fission barrier) is shown, which is by far not the case for vibrational zero-point motion energies. It is fair to assume that the latter energies should indeed modify the absolute value of the energy, but should produce in average an elongation dependence close to zero if one includes all the relevant dynamical collective modes (elongation as well as those perpendicular to the fission mode). One should also note that, even though we have considered (near the second fission barrier) solutions which break the intrinsic parity, they do not correspond to good parity states. Upon projecting onto the positive parity, one would get some extra correction which should add up (with the same sign as it is shown in, *e.g.*, ref. [51]) to the one coming from the intrinsic solution. Such a symmetry restauration study is currently undertaken. The potential energy landscape is rather complicated in the descent to scission (significantly after the second saddle point), see, *e.g.*, refs. [3] and [9]. As such, it is beyond the scope of our calculations to explore

the relevant collective modes amounting at least to the variation of five independent parameters (see [3]). Therefore, the strategy should be first to check the relevance of phenomelogical approaches with respect to ours, then, the latter being validated, to exploit their results to select some regions of interest in the collective deformation space. This is presently performed to study the spins of fission fragments at low energy (as, *e.g.*, the spontaneous fission of ^{252}Cf) within the orientation pumping approach of ref. [52], using microscopic wave functions at whatever configuration which could be deemed as a reasonable scission configuration for a given (N_1, Z_1 and N_2, Z_2) fragmentation.

We are indebted to G. Barreau, J. Libert, H. Goutte, M. Girod and P. Möller for interesting discussions. One of the author (Ph. Q.) would like to thank the Theoretical Division of the LANL (Los Alamos) for the warm hospitality extended to him during fruitful visits.

References

1. V.M. Strutinsky, Nucl. Phys. A **95**, 420 (1967); **122**, 1 (1968).
2. P. Möller, J.R. Nix, in *Proceedings of the IAEA Symposium on Physics and Chemistry of Fission, Rochester, 1973*, Vol. **I** (IAEA, Vienna, 1974) p. 103.
3. P. Möller, D.G. Madland, A.J. Sierk, A. Iwamoto, Nature **409**, 785 (2001).
4. J. Maruhn, W. Greiner, D. Drechsel, in *Proceedings of the IAEA Symposium on Physics and Chemistry of Fission, Rochester, 1973*, Vol. **I** (IAEA, Vienna, 1974) p. 569.
5. M. Brack, J. Damgaard, A.S. Jensen, H.C. Pauli, V.M. Strutinsky, C.W. Wong, Rev. Mod. Phys. **44**, 320 (1972).
6. V.V. Pashkevich, Nucl. Phys. A **133**, 400 (1969).
7. S.E. Larsson, I. Ragnarsson, S.G. Nilsson, Phys. Lett. B **38**, 269 (1972).
8. U. Götz, H.C. Pauli, K. Junker, Phys. Lett. B **39**, 436 (1972).
9. V.V. Pashkevich, in *Proceedings of the 15th Divisional Conference on Low-Energy Nuclear Dynamics, St. Petersburg, Russia, 1995* (World Scientific, Singapore, 1995) p. 161.
10. H. Flocard, P. Quentin, D. Vautherin, M. Véneroni, A.K. Kerman, Nucl. Phys. A **231**, 176 (1974).
11. J. Bartel, P. Quentin, M. Brack, C. Guet, H.-B. Håkansson, Nucl. Phys. A **386**, 79 (1982).
12. J.-F. Berger, M. Girod, D. Gogny, Nucl. Phys. A **502**, 85c (1989).
13. H. Goutte, J.F. Berger, private communication.
14. J.H. Huizenga, R. Vandenbosch, in *Nuclear Fission* (Academic Press, New York, 1973).
15. S. Bjørnholm, J. Lynn, Rev. Mod. Phys. **52**, 725 (1980).
16. H. Weigmann, in *The Nuclear Fission*, edited by C. Wagemans (CRC Press, Boca Raton, 1991) Chapt. II.
17. G.N. Smirenkin, IAEA Report INDC(CCP)-359 (1993).
18. K. Rutz, J. Maruhn, P.G. Reinhard, W. Greiner, Nucl. Phys. A **590**, 680 (1995).
19. A.V. Affanassyev, P. Ring, Acta Phys. Hung. **13**, 139 (2001).
20. M. Warda, J.L. Egido, L.M. Robledo, K. Pomorski, Phys. Rev. C **66**, 014310 (2002).
21. H. Flocard, P. Quentin, A.K. Kerman, D. Vautherin, Nucl. Phys. A **203**, 433 (1973).
22. D. Samsœn, P. Quentin, J. Bartel, Nucl. Phys. A **652**, 34 (1999).
23. H. Krivine, O. Bohigas, J. Treiner, Nucl. Phys. A **366**, 155 (1980).
24. M. Beiner, H. Flocard, N. Van Giai, P. Quentin, Nucl. Phys. A **238**, 29 (1975).
25. M. Brack, C. Guet, H.-B. Håkansson, Phys. Rep. **123**, 275 (1985).
26. J. Libert, M. Meyer, P. Quentin, Phys. Rev. C **25**, 586 (1982).
27. N. Pillet, P. Quentin, J. Libert, Nucl. Phys. A **697**, 141 (2002).
28. M. Meyer, J. Libert, P. Quentin, Phys. Lett. B **95**, 175 (1980).
29. H. Laftchiev, D. Samsœn, P. Quentin, J. Piperova, Eur. Phys. J. A **12**, 155 (2001).
30. T.L. Ha, P. Quentin, D. Strottman, in preparation.
31. S.J. Krieger, P. Bonche, H. Flocard, P. Quentin, M.S. Weiss, Nucl. Phys. A **517**, 275 (1990).
32. H.J. Lipkin, Ann. Phys. (N.Y.) **9**, 272 (1960).
33. I. Kelson, Y. Shoshani, Phys. Lett. B **40**, 58 (1972).
34. S.D. Belyaev, Nucl. Phys. **24**, 322 (1961), and references quoted therein.
35. D.W.L. Sprung, S.G. Lie, M. Vallières, P. Quentin, Nucl. Phys. A **326**, 37 (1979).
36. D.J. Thouless, J.G. Valatin, Nucl. Phys. **31**, 211 (1962).
37. J. Libert, M. Girod, J.P. Delaroche, Phys. Rev. C **60**, 054301 (1999).
38. P. Quentin, H. Lafchiev, D. Samsœn, I.N. Mikhaïlov, Phys. Rev. C **69**, 054315 (2004).
39. M.J. Giannoni, P. Quentin, Phys. Rev. C **21**, 2076 (1980).
40. P. Ring, P. Schuck, in *The Nuclear Many-Body Problem* (Springer Verlag, 1980) Chapt. 11.
41. W.H. Bassichis, A.K. Kerman, J.P. Svenne, Phys. Rev. **160**, 746 (1967).
42. H. Flocard, P. Quentin, D. Vautherin, M. Veneroni, A.K. Kerman, Nucl. Phys. A **231**, 176 (1974).
43. P. Reiter *et al.*, Phys. Rev. Lett. **82**, 509 (1999).
44. J.L. Egido, L.M. Robledo, Phys. Rev. Lett. **85**, 1198 (2000).
45. T. Duguet, P. Bonche, P.H. Heenen, Nucl. Phys. **679**, 427 (2001).
46. H. Laftchiev, D. Samsœn, P. Quentin, J. Piperova, Eur. Phys. J. A **12**, 155 (2001).
47. D. Hoffman, Nucl. Phys. A **502**, 21c (1989).
48. H.X. Zhang, T.R. Yeh, H. Lancman, Phys. Rev. C **34**, 1397 (1986).
49. J. Blons, B. Fabbro, C. Mazur, D. Paya, M. Ribrag, Y. Patin, Nucl. Phys. A **477**, 231 (1988).
50. P.H. Heenen, private communication.
51. P. Bonche, S.J. Krieger, M.S. Weiss, J. Dobaczewski, H. Flocard, P.-H. Heenen, Phys. Rev. Lett. **66**, 871 (1991).
52. I.N. Mikhaïlov, P. Quentin, Phys. Lett. B **462**, 7 (1999).